iScience

CellPress
OPEN ACCESS

Article

FGF9 is required for Purkinje cell development and function in the cerebellum

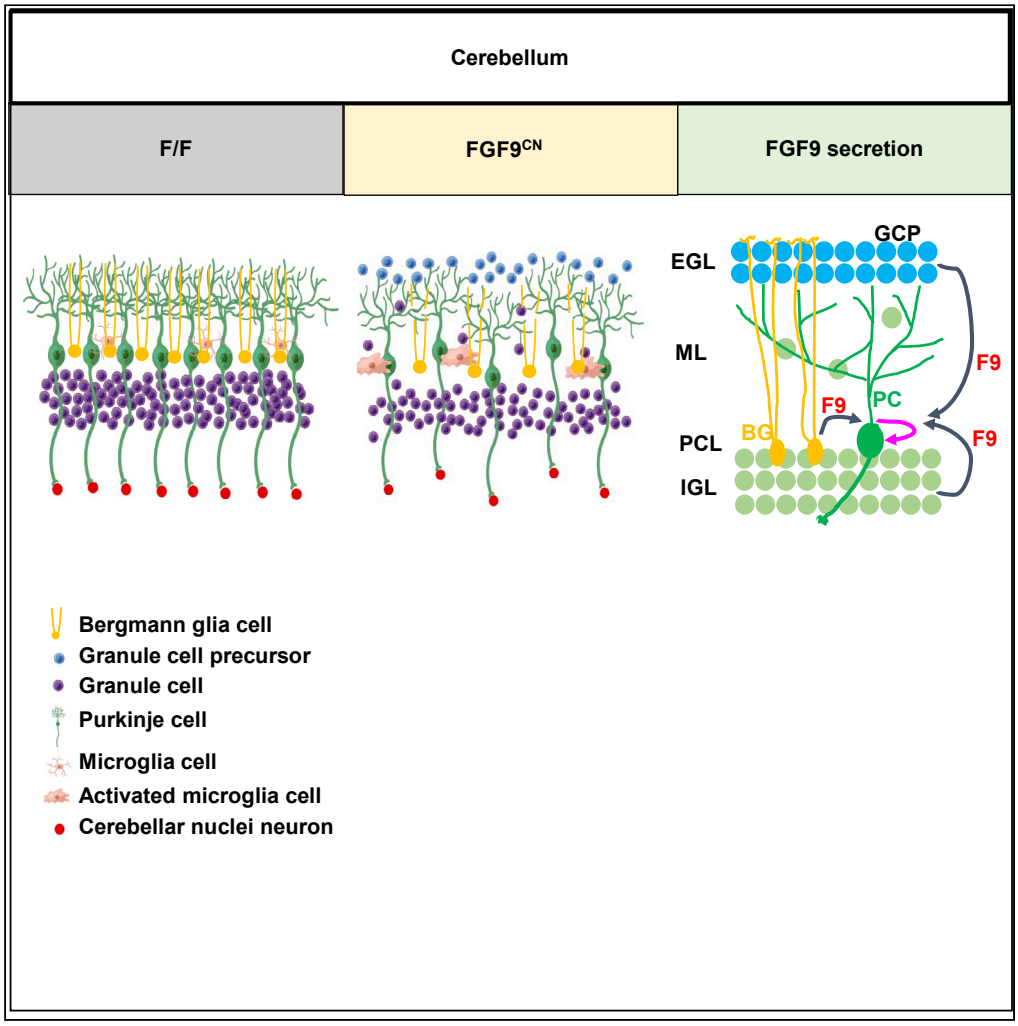

Ping He, Shuting Zhong, Shuaijun Lin, ..., Xiaokun Li, Peijun Li, Cong Wang

pjl72@hotmail.com (P.L.)
cwang@wmu.edu.cn (C.W.)

Highlights

FGF9 maintains mouse motor function via regulating Purkinje cell development

Ablation of FGF9 disrupts the intrinsic excitation of Purkinje cells

FGF9 deletion affects cerebellar neurotransmitter release

FGF9 deficiency leads to neuronal injury and inflammation in cerebellum

He et al., iScience 27, 109039
February 16, 2024
https://doi.org/10.1016/j.isci.2024.109039

iScience

CellPress
OPEN ACCESS

Article

FGF9 is required for Purkinje cell development and function in the cerebellum

Ping He,[1] Shuting Zhong,[1] Shuaijun Lin,[1] Zhiyan Xia,[1] Liqing Wang,[1] Yuhe Han,[1] Di Xu,[2] Shuping Hu,[1] Xiaokun Li,[1] Peijun Li,[2,3,*] and Cong Wang[1,4,*]

SUMMARY

Fibroblast growth factor 9 (FGF9) is a member of the fibroblast growth factor family, which is widely expressed in the central nervous system (CNS). It has been reported that deletion of FGF9 leads to defects in cerebellum development, including Purkinje cell defect. However, it is not clear how FGF9 regulating cerebellar development remains to be determined. Our results showed that in addition to disrupt Bergmann fiber scaffold formation and granule neuron migration, deletion of neuronal FGF9 led to ataxia defects. It affected development and function of Purkinje cells, and also changed the action potential threshold and excitation frequency. Mechanistically, depletion of FGF9 significantly changed neurotransmitter contents in Purkinje cells and led to preferential increase in inflammation, even downregulation in ERK signaling. Together, the data demonstrate that neuronal FGF9 is required for the development and function of Purkinje cells in the cerebellum. Insufficient FGF9 during cerebellum development will cause ataxia defects.

INTRODUCTION

The cerebellum as a major part of the hindbrain helps precisely coordinating body movement and balance.[1] During cerebellum development, postmitotic granule cells of the external granular layer (EGL) migrate radially through the molecular layer (ML) to settle in the internal granular layer (IGL) which is an important activity for cerebellar development.[2] Bergmann glia (BG) are unipolar glial cells situated aligning to the Purkinje cell layer (PCL), with radial fibers passing through the ML and providing guidance for granule cell migration and forming synapses with the dendrites of Purkinje cells.[3] Purkinje cells derived from the ventricular zone are one kind of GABAergic inhibitory neurons, which receive modulatory input from extensive parallel fibers and climbing fibers that arise in the inferior olive. After the excitatory input has been analyzed and integrated, the Purkinje cells directly project inhibitory signals in turn to the neurons in the deep cerebellar nuclei.[4] Thus, pathological changes in Purkinje neurons are closely associated with the congenital ataxia symptoms.

Ataxia is a crippling nervous system disease etiologically induced by a combination of hereditary and environmental variables, which causes limb movement autonomous dysfunction.[5] Abundant evidence extensively suggests that genetic factors have a close relationship with ataxia occurrence named.[6] As the genetically heterogeneous disorder, hereditary ataxias can be inherited in three different ways including autosomal dominant, autosomal recessive and X-linked manner, in which the incidence rate of autosomal recessive cerebellar ataxia (ARCA) reaches approximately 3/10000 accompanied with similar symptoms such as cerebellar atrophy or hypoplasia.[3] Purkinje cell dysfunction or degeneration is frequently found in patient and animal models with cerebellar ataxia.[7–9] Although ARCA patients have severe impairment, what we know is still very limited of its elusive mechanism and specific treatment.[1,6,7]

Aberrant FGF signaling causes defects in brain and cerebellum development.[8] Among the 18 receptor-binding FGFs, FGF7, FGF8, FGF9, FGF10, FGF14, FGF17, FGF18, and FGF22 are expressed in the cerebellum at different developmental stages.[9–11] It has shown that FGF2 secreted by astrocytes interacts with neuronal FGFR1 to maintain synaptogenesis for supporting prenatal neurogenesis.[12] FGF8 transcripts observed in the EGL at E16.5 and P0 mice are significantly decreased at Postnatal 7 days. Moreover, mutation in regulator of Gli signaling dramatically accelerates FGF8 expression in EGL.[13,14] FGF9 expression first appeared in cerebellum at E16.5 which is predominantly expressed in neurons and functions as a glia-activating factor (GAF) to promote the differentiation and survival of neurons and glia in the central nervous system (CNS).[15] FGF9 ablation in GABAergic neurons caused severe ataxia via significantly affecting the survival and development of Purkinje cells.[16] It has been reported specifically knockout *Fgf9* in mouse with Nestin-Cre driver causes severe ataxia which demonstrated the control activity of granule neurons derived FGF9 in the formation of Bergmann fiber scaffold.[2] However, Nestin as a neural stem cell/progenitor cell specific protein is descended inducing by cell differentiation.[17] In addition to neuronal cells, Nestin also expresses in many other embryonic tissues. Therefore, whether other cell-derived FGF9 also plays a role in cerebellum development is not fully addressed. Although it has

[1]School of Pharmaceutical Sciences, Wenzhou Medical University, Wenzhou 325030, Zhejiang, China
[2]Department of Neurology, Institute of Geriatric Neurology, the Second Affiliated Hospital and Yuying Children's Hospital Wenzhou Medical University, Wenzhou 325027, Zhejiang, China
[3]Key Laboratory of Structural Malformations in Children of Zhejiang Province, Wenzhou 325027, Zhejiang, China
[4]Lead contact
*Correspondence: pjl72@hotmail.com (P.L.), cwang@wmu.edu.cn (C.W.)
https://doi.org/10.1016/j.isci.2024.109039

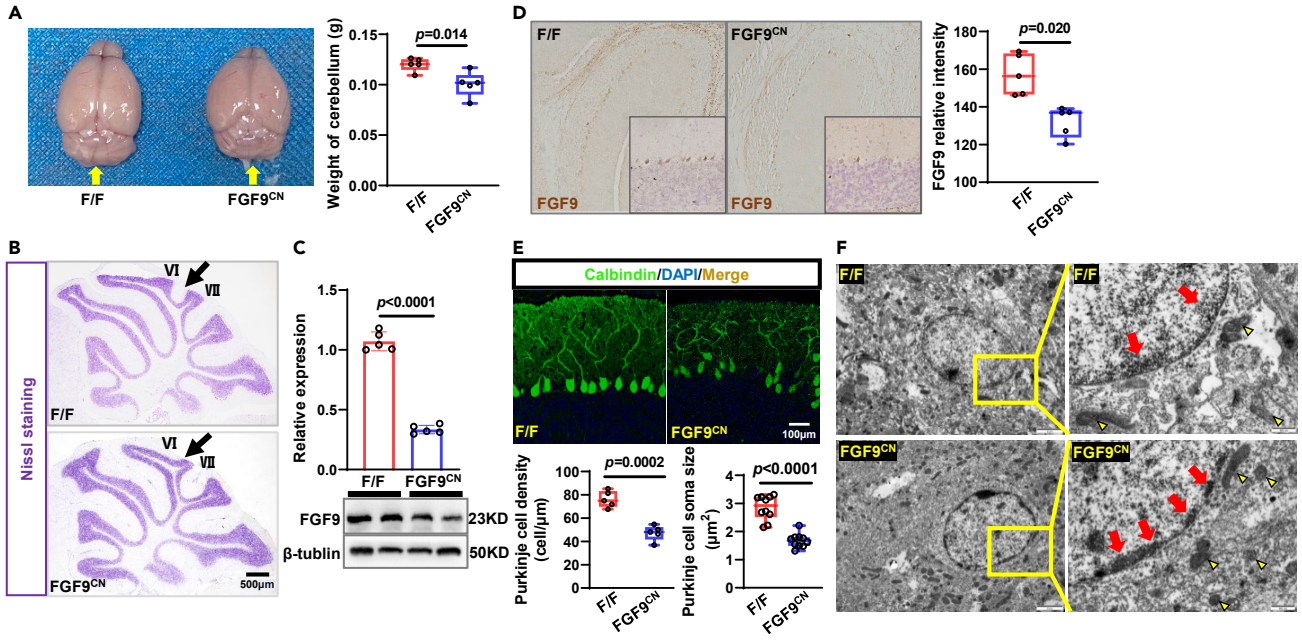

Figure 1. Granule and Bergmann cell derived FGF9 is essential for Purkinje cell development

(A) Representative cerebellar images (left) and cerebellar weight quantification (right) in *Fgf9*$^{f/f}$ and *Fgf9*^{cnGFAP} mice (n = 5).

(B) Nissl staining showing the changes of cerebellum lobes of 3m *Fgf9*$^{f/f}$ and *Fgf9*^{cnGFAP} mice.

(C) Q-PCR and Western blotting show decreased FGF9 expression (n = 5), β-actin was used as a loading control.

(D) Immunohistochemistry shows decreased FGF9 expression in *Fgf9*^{cnGFAP} mice (n = 5).

(E) Immunofluorescence staining detecting Calbindin (Green) positive Purkinje cells in mouse cerebellum. ImageJ analyses (below panels) of Purkinje cell density (n = 5) and cell soma size (n = 10). DAPI for the counterstaining of nucleus.

(F) The ultrastructure of Purkinje cells in control and *Fgf9*^{cnGFAP} cerebellum, red arrows indicate chromatin and yellow arrows as mitochondria. Data are represented as Mean ± SD. Statistical analysis was performed using the unpaired two-tailed Student's *t* test. *, p < 0.05; F/F, *Fgf9*$^{f/f}$ control mice; FGF9^{CN}, *Fgf9*^{cnGFAP} mice.

been reported that ablation of FGF9 in Bergmann and glia cells with GFAP-Cre leads to Purkinje cell misalignment, no thorough characterization of the defects has been reported.[2]

To determine the role of local paracrine FGF9 in Purkinje cell development, we thoroughly characterized Purkinje proliferation, interaction with Bergmann fibers during migrations, and neuronal signaling transmission in GFAP-Cre mediated FGF9 conditional null (*Fgf9*^{cnGFAP}) mice that has glia and neurons specific FGF9-ablation. We demonstrated that FGF9 deletion in glia and neurons affected Purkinje cells development and function and caused typical ataxia defects in mice, which indicated that FGF9 played important roles in keeping the homeostasis of movement.

RESULTS

Granule and Bergmann cell derived FGF9 is essential for Purkinje cell development

Previous report shows that ablation of FGF9 alleles in the granule cells and Bergmann glia with GFAP-Cre (designated *Fgf9*^{cnGFAP}) leads to ataxia phenotype in mice.[2] However, the detailed phenotype remains to be characterized. To address this issue, the brain of 12 weeks of *Fgf9*^{cnGFAP} mice was dissected. Gross morphology showed that the *Fgf9*^{cnGFAP} cerebellum was smaller than that of wildtype control (Figure 1A). The intercrural fissure between lobules VI and VII was absent in *Fgf9*^{cnGFAP} mice (Figure 1B). We then assessed the effect of FGF9 on Purkinje cell arrangement and morphology after FGF9 expression was specially decreased in cerebellum, which was indicated by mRNA and protein detection (Figures 1C and 1D). Consistent with the previous report, three-month old *Fgf9*^{cnGFAP} cerebellum showed that disrupted Bergmann fiber scaffold formation, impaired granule neuron migration, and upset Purkinje cell alignment and maturation. Both the density and soma size of Purkinje cells were reduced, which indicated the impaired dynamics of synaptogenetic and of synaptic stabilization processes (Figures S1A, S1B, and 1E). Furthermore, transmission electronic microscopy of Purkinje soma showed accumulation of swollen mitochondria, abundant autophagosome, lysosomes, and perinuclear chromatin, signs of early apoptosis (Figure 1F).

Unlike ablation of FGF9 in all neuron cells with Nestin-Cre, *Fgf9*^{cnGFAP} mice did not have typical ataxic gait (Figure 2A). However, the mice still showed paroxysmal hyperextended hind limbs with chronic spasms (Figure 2B), a typical ataxic phenotype. Generally, *Fgf9*^{cnGFAP} mice were a little bit smaller than control mice at the same age but without significant difference (Figure 2C). Furthermore, other ataxic behavioral experiments, such as rotation rod and balancing beam were used to evaluate the locomotor coordination defects in *Fgf9*^{cnGFAP} mice

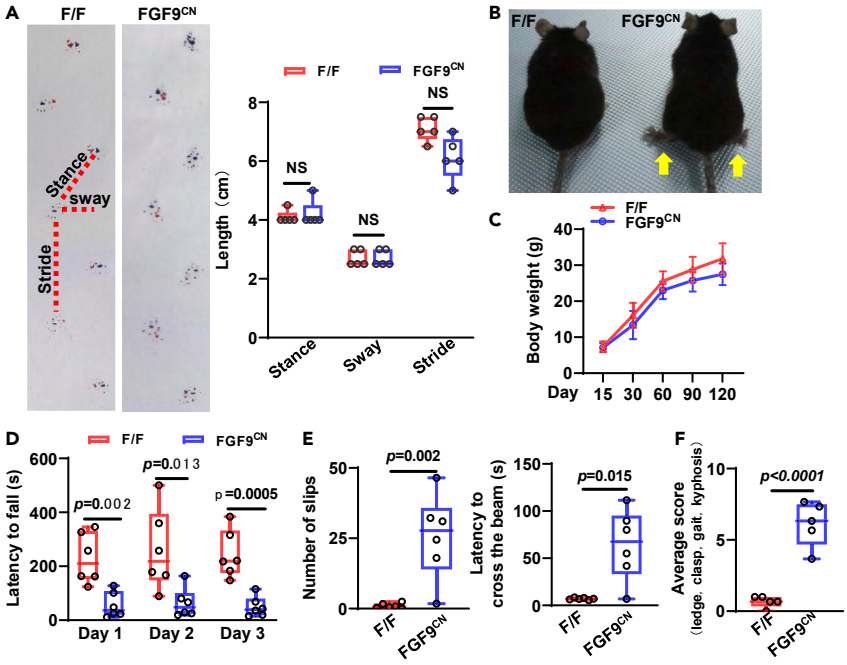

Figure 2. Ablation of FGF9 provokes the characteristic of ataxia

(A) Assessment of gait using footprint test (n = 5). Red ink indicating the forefoot print and blue ink the rear footprint. The length of stance, sway, stride of mouse footprint was quantitated on the right panel.

(B) *Fgf9*^{cnGFAP} mice have paroxysmal hyperextended hind limbs with chronic spasms. The yellow arrows showing extended outward of hind limbs.

(C) *Fgf9*^{cnGFAP} mice exhibit growth retardation from postnatal day 30 (n = 8). Data represent Means ± SD, Statistical analysis was performed using two-way ANOVA followed by Tukey's post hoc test.

(D) Quantification of the latency to fall in the rotarod test (n = 6). Data for the 3 days of evaluation are shown.

(E) The measurement of foot slips and the latency to traverse the balance beam (n = 6).

(F) Mice were assessed on a 0–3 scale each for ledge test, clasping, gait, and kyphosis (n = 5). Average composite score for each genotype was calculated. Data are represented as Mean ± SD. Statistical analysis was performed using the unpaired two-tailed Student's *t* test. *, p < 0.05; F/F, *Fgf9*$^{f/f}$ control mice; FGF9^{CN}, *Fgf9*^{cnGFAP} mice.

(Figures 2D and 2E). Quantification analyses showed that *Fgf9*^{cnGFAP} mice had had significant reduced latency of falling from the rotated rod (Figure 2D), higher foot slips and the time to across the beam (Figure 2E) than did the control mice. Overall, the composite phenotype score of ataxias showed that the *Fgf9*^{cnGFAP} was a significantly higher than the control mice (Figure 2F).

Ablation of FGF9 leads to disassociation of Purkinje cells from climbing fibers

Consistent with previous report ablation of FGF9 led to cerebellum development defects, as demonstrated by H&E and immunofluorescence staining with Purkinje cell-specific antibody calbindin (Figures S1A and S1B), in the adult cerebellum, dendritic fibers and soma of Purkinje cells are closely intertwined with the fibers ascending from the lower olive nucleus of the medulla oblongata to the ML. Purkinje cell-specific calbindin staining and glutamatergic nerve terminals-specific VGlut2 staining revealed that the proximal dendritic tree of the Purkinje cells aligned smoothly and largely covered by the terminal of a single climbing fiber (Figure 3A). Unlike control cerebellum where the Purkinje cells and climbing fibers was overlapping, the Purkinje cells are poorly aligned and not fully overlapped with climbing fiber in *Fgf9*^{cnGFAP} cerebellum. However, abundant climbing fibers still existed in adult *Fgf9*^{cnGFAP} cerebellum (Figures 3B and 3C). Interestingly, parallel fiber-specific VGlut1 staining showed that no obvious difference of VGlut1+ parallel fibers between control and *Fgf9*^{cnGFAP} cerebella (Figure 3D). In addition, we investigated neuronal maturation via double staining with DCX and NeuN, respectively as immature and mature neuron markers. The results suggested that FGF9 deletion led to more than two-fold increase in the ratio of DCX to NeuN positive granule cells, which indicating the delayed granular cell maturation except presenting in post-migratory Purkinje cells (Figure 3E).

Ablation of FGF9 leads to overexcitation and irregular action potentials in Purkinje cells

Purkinje cell activity is the sole output of the cerebellar cortex.[18] To determine whether ablation of FGF9 changed Purkinje cell electrophysiology, we performed Purkinje cell attached recorder to document excitation signals. We observed that the Purkinje cells in the cerebellum of *Fgf9*^{cnGFAP} mice were overexcited with a lower action potential threshold accompanied with the step by step increase of depolarizing current (Figures 4A and 4B). The spontaneous recording results showed that the spontaneous firing frequency of Purkinje cells in *Fgf9*^{cnGFAP} mice was

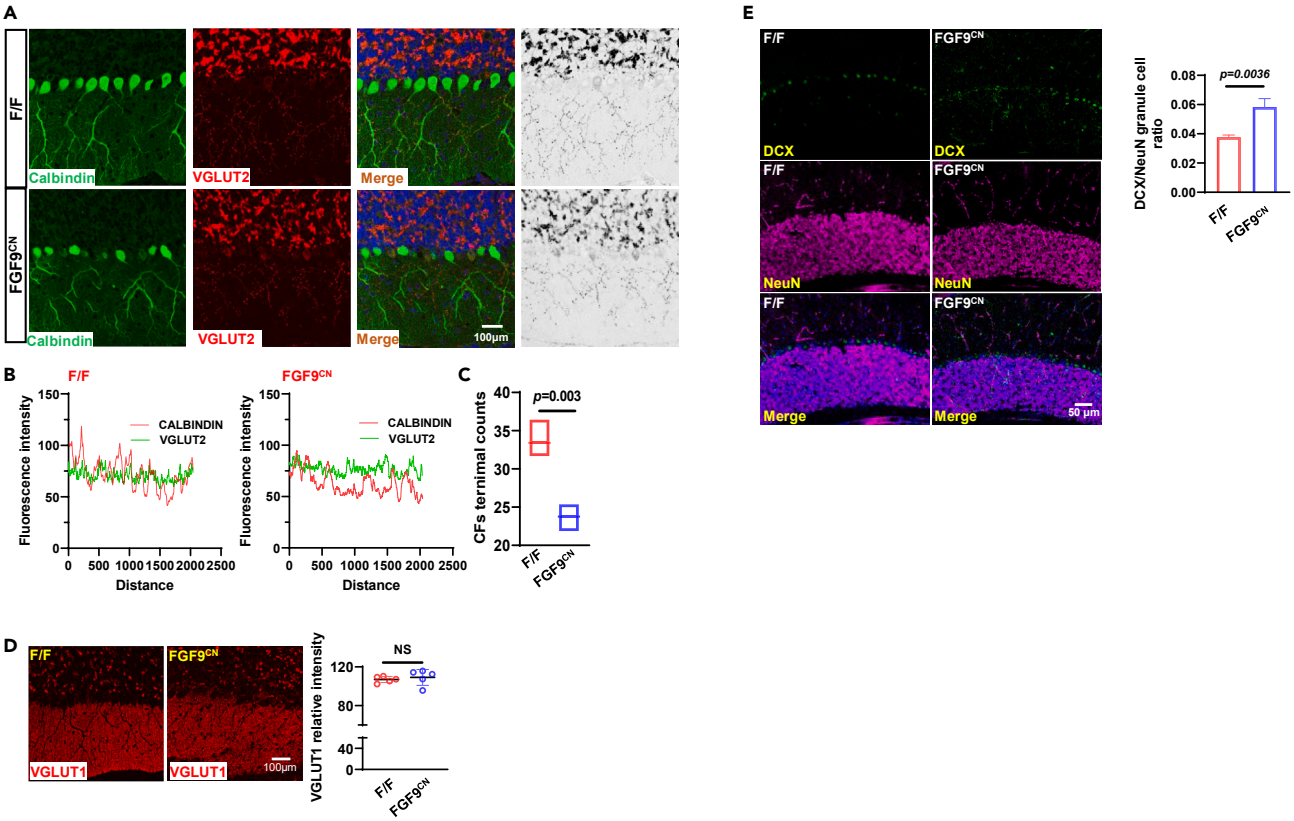

Figure 3. Ablation of FGF9 leads to disassociation between Purkinje cells from climbing fibers

(A) Double immunofluorescence staining analyzing the expression of Calbindin (Green) and VGlut2 (Red) in adult mouse cerebella (n = 5). Nuclei were counterstained with DAPI (blue).

(B) Colocalization and relative protein expression of Calbindin and VGlut2 analyzed by ImageJ software (n = 5).

(C) Climbing fiber (CF) terminals counts analyzed by ImageJ.

(D) Immunofluorescence staining of VGlut1 showing parallel fibers (n = 5). ImageJ quantitates the fluorescence intensity.

(E) Double immunofluorescence staining analyzing the expression of DCX (Green) and NeuN (Red) in adult mouse cerebella (n = 5). Immature/mature granule cell ratio was analyzed by ImageJ. Data are represented as Mean ± SD. Statistical analysis was performed using the unpaired two-tailed Student's *t* test. *, $p < 0.05$; F/F, *Fgf9*$^{f/f}$ control mice; FGF9^{CN}, *Fgf9*^{cnGFAP} mice.

less frequent (p = 8, n = 13) comparing to that of wildtype control mice (Figure 4C). Moreover, the firing of Purkinje cells in *Fgf9*^{cnGFAP} mice showed more irregular pattern, evidenced by the non-consistent inter-spike intervals. To examine the excitability of the Purkinje cells, whole cell recordings were performed under current clamp mode. Notably, morphological images of Purkinje cells filling with Biocytin-dye were captured by confocal during whole cell recording (Figure 4D).

FGF9 deficiency affects neurotransmitter abundance in cerebellum

To investigate how deficient in FGF9 affected neurotransmitters production the cerebellum, quantitative LC-MS/MS with MRM analyses were used to compare neurotransmitters in the control and *Fgf9*^{cnGFAP} cerebella, which included a total of 30 targeted molecules (Table 1). It was clear that the abundance of neurotransmitter in the *Fgf9*^{cnGFAP} cerebellum was different from the control mice (Figure 5A). Among them, 5-hydroxyl-Ltryptophan, 5-HAA, dopamine, homovanillic acid (HVA) and 3,4-Dihydroxyphenylacetate (DOPAC) were increased, whereas 3,4-Dihydroxymandelic acid (DOMA) was decreased (Figure 5B). HVA and 5-HAA are involved in dopaminergic and serotoninergic neuronal activities. Thus, high levels of HVA and 5-HAA likely underpin the movement defects in *Fgf9*^{cnGFAP} mice.

Ablation of FGF9 leads to mild neuroinflammation

In order to investigate the inflammatory reaction in cerebellum, quantitative RT-PCR analysis was used to detect myelination correlated with CNS disease, which showed a decrease in myelin expression at the mRNA level in the cerebellum of postnatal 7-day mice (Figure 6A). FGF9 deletion significantly promoted the expression of proinflammatory factors in the cerebellum compared to the cerebral cortex (Figure S2), which guided us to figure out how FGF9 ablation facilitated neuroinflammation in the cerebellum. Therefore, immunostaining for ionized

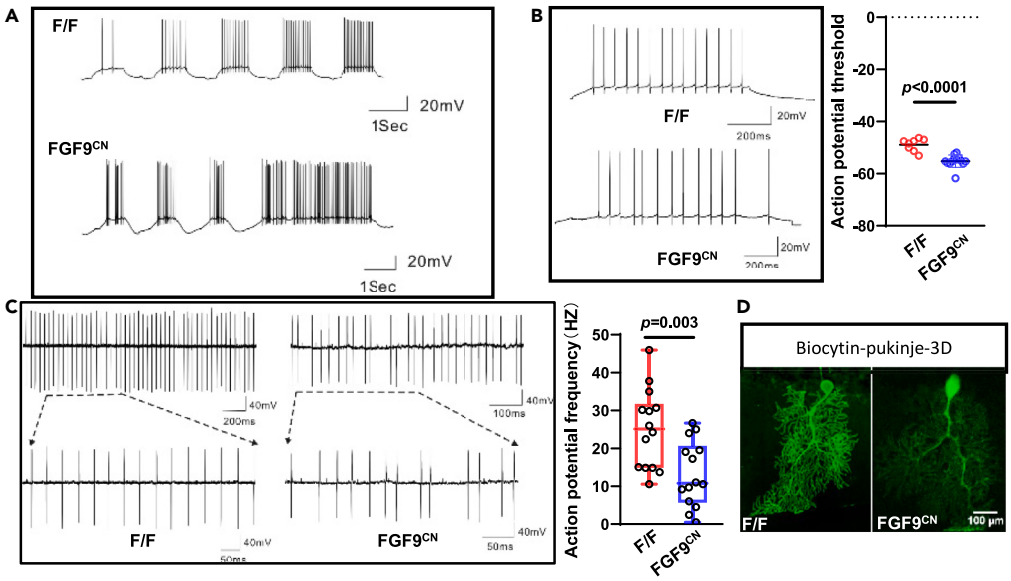

Figure 4. FGF9 deletion stimulates higher excitation of Purkinje cells

(A) Action potential firing patterns of Purkinje cells recorded with different steps of depolarization under current clamp mode (n = 14).

(B) Representative traces of action potential firing pattern in control (up panel) and *Fgf9*^{cnGFAP} (below panel) purkinje cells (n = 14). Statistical analysis of action potential threshold (right panel).

(C) Representative traces cell attached recording of spontaneous action potential firing in control (up panel) and *Fgf9*^{cnGFAP} (below panel) Purkinje cells (n = 14). Irregular firing observed in FGF9 deletion Purkinje cells. Lower frequency of action potential was indicated in FGF9 deletion group (right).

(D) Confocal image of a biocytin filled Purkinje cell in the cerebellum of control group (scale 50 μm, n = 10). Data are represented as Mean ± SD. Statistical analysis was performed using the unpaired two-tailed Student's *t* test. *, p < 0.05; F/F, *Fgf9*$^{f/f}$ control mice; FGF9^{CN}, *Fgf9*^{cnGFAP} mice.

calcium binding adaptor molecule 1 (IBA1), a 17-kDa protein upregulated in microglia following nerve injury, was carried out to assess neuroinflammation in *Fgf9*^{cnGFAP} cerebellum via assessing IBA1 expression. It was clear that expression of IBA1 increased in the cerebella of 3-month-old *Fgf9*^{cnGFAP} mice (Figures 6B and 6D). To investigate whether FGF9 deletion influenced the radial glial scaffold, Calbindin and GFAP double staining were applied to determine the Bergmann glial fiber development. At adult stage, GFAP positive cell with a stellate morphology were found in the ML of *Fgf9*^{cnGFAP} cerebellum, which completely lost their unipolar/bipolar morphology (Figure 6C). Meanwhile, Western blotting indicated the protein expression of GFAP remarkably accumulated in *Fgf9*^{cnGFAP} cerebellum, while the phosphorylation of ERK was downregulated after FGF9 deletion, which was the downstream of FGF signaling (Figure 6D). In addition, Rhodamine-123 staining of primary astrocytes extracted from cerebellum suggested that FGF9 deficiency led to mitochondrial dysfunction through decreasing the mitochondrial membrane potential of astrocytes (Figure S3A). Immunofluorescence staining showed that addition of FGF9 rescue the asteroid cell morphology in *Fgf9*^{cnGFAP} glial cells, just like the control glia (Figure S3B). The results suggest that ablation of FGF9 leads to neuronal injury and inflammation in cerebellum via interrupting FGF signaling, which is consistent with the results that FGF9 deficiency lowers myelin expression in cerebellum.

DISCUSSION

FGF9 originally described as glia-activating factor predominantly expressed in the nerve system and processes broad biological activities.[2,19] It has reported that FGF9 secreted from granule neurons and controls framework arrangement of spiral strands and internal movement. Highly expressed FGF9 was evident both in granule cell precursors in the EGL at birth and in most granule cells completing their migration to the IGL at P7, while interestingly, FGF9 transcripts were detected primarily in PCs at P21.[13] The function of FGF9 in altering the fate of neural progenitor cells is mostly through increasing proliferation and inhibiting astrocyte and oligodendrocyte differentiation.[20] Deletion of FGF9 in glia and neurons leads to impairment of limb motor coordination and loss of Purkinje cells, the phenotypes presented in ataxia.[2,21] Unfortunately, the vivo effects of FGF9 in general have not been fully clarified. Herein, we discovered that ablation of neuronal FGF9 caused ataxic defects, affected development and function of Purkinje cells, changed the action potential threshold and excitation frequency of Purkinje cell, and altered neurotransmitter contents in Purkinje cells. In addition, it not only disrupted formation of Bergmann fiber scaffold but also migration of granule neuron as reported previously.

In the present study, we firstly have established that the mRNA and protein level of FGF9 reduced in cerebellum after specific knockout of FGF9, which leads to the morphological and functional changes of cerebellum especially the malalignment of Purkinje cells. The cerebellar cortex is composed of three structurally distinct layers, ML, the PCL and the granular layer (GL) (Figure 7A). ML as the most superficial layer

Table 1. The concentrations of neurotransmitters registered in cerebellum

Metabolite Name	F/F	$FGF9^{CN}$
Serine	1.81818 ± 0.18488	2.27219 ± 0.08418*
DL-Norepinephrine	0.10780 ± 0.03245	0.17822 ± 0.01962*
Serotonin (5-HT)	0.01300 ± 0.00169	0.03101 ± 0.01020*
Arginine	0.16949 ± 0.02274	0.26964 ± 0.05529*
Tryptophan	0.06829 ± 0.00924	0.10285 ± 0.01920*
Histamine	0.00003 ± 0.00002	0.00015 ± 0.00008*
5-Hydroxy-L-tryptophan	0.00053 ± 0.00014	0.00113 ± 0.00038*
5-Hydroxyindole-3-acetic acid (5-HIAA)	0.00119 ± 0.00039	0.00234 ± 0.00072*
3,4-Dihydroxymandelic acid (DOMA)	0.00256 ± 0.00037	0.00157 ± 0.00066*
Dopamine	0.00442 ± 0.00184	0.02439 ± 0.01543*
Homovanillic acid (HVA)	0.00094 ± 0.00052	0.00333 ± 0.00180*
3,4-Dihydroxyphenylacetate (DOPAC)	0.01915 ± 0.00609	0.04077 ± 0.01624*
Phenylalanine	0.29633 ± 0.01280	0.32534 ± 0.02271
Glutamate	5.78459 ± 0.10620	5.39639 ± 0.35438
Tryptamine	0.000003 ± 0.00000	0.00001 ± 0.00000
Ornithine	0.00108 ± 0.00004	0.00174 ± 0.00079
Tyrosine	5.49734 ± 0.74548	7.01691 ± 1.83415
Normetanephrine	0.08182 ± 0.00956	0.10266 ± 1.02837
Ethanolamine	0.13344 ± 0.00145	0.14361 ± 0.01640
Rac4-Hydroxy-3-methoxyphenylethylene	0.00126 ± 0.00024	0.00156 ± 0.00044
Glycol (MHPG)	0.00002 ± 0.00001	0.00002 ± 0.00001
Phenylethylamine	0.00143 ± 0.00068	0.00228 ± 0.00123
3-Methoxytyramine hydrochloride	0.00050 ± 0.00006	0.00170 ± 0.00232
Tyramine	0.00086 ± 0.00042	0.00062 ± 0.00023
3-Methoxy-4-hydroxymandelate (VMA)	11.58317 ± 0.24033	12.25616 ± 1.59777
Glutamine	0.13629 ± 0.01235	0.15138 ± 0.04123
4-Aminobutyric acid (GABA)	0.00018 ± 0.00003	0.00021 ± 0.00007
N-acetyl serotonin	0.01323 ± 0.00229	0.01433 ± 0.00521
3,4-Dihydroxyphenylethyleneglyco (DHPG)	1.30159 ± 0.09971	1.32157 ± 0.04264
Threonine	0.00001 ± 0.00000	0.00001 ± 0.00000
5-Methoxytryptamine		
3-Hydroxyanthranilic acid		
Levodopa (DOPA)		
Epinephrine		

*$P < 0.05$.

hosts basket cells, stellate cells and Purkinje cell dendrites, in which with low-density cell population and high synaptic occurrence.[22] In the PCL, the main bodies of Purkinje cells surrounded by multiple Bergmann glia cell are located and send their axon to the deep nuclei crossing the GL.[23,24] The GL is the deepest layer with the highest cell density, in which contains a large number of granule cells, interneuron like unipolar brush cell (UBCs) and Golgi cells.[22,25] Our study indicated that GFAP expressed by activated astrocyte dramatically ascended in the ML of FGF9 knockout cerebellum. Consistent with this, we found IBA1, a well-established marker for microglia/macrophages, raised in ML after FGF9 deletion. The results suggested that FGF9 activity acted as a negative modulator of neuroinflammation in cerebellum. Moreover, our investigation determined that FGF9 depletion inhibited the maturation of granule cells via staining with DCX, however, post-migratory Purkinje cells in PCL were also positive stained which is similar with data already reported.[26]

A previous study has highlighted the roles of FGFR signal in the neurogenesis. Coincident with it, our present study has detected the downstream pathway of FGF and showed that FGF9 ablation led to the shrinkage of ERK phosphorylation. Additionally, we demonstrate here that the *Fgf9*^{cnGFAP} cerebellum had less Purkinje cells than control littermates, which were poorly aligned. In addition, the primary Purkinje cell dendrites were elongated after FGF9 deletion, whereas the secondary dendrite numbers were decreased. It is plausible that FGF9

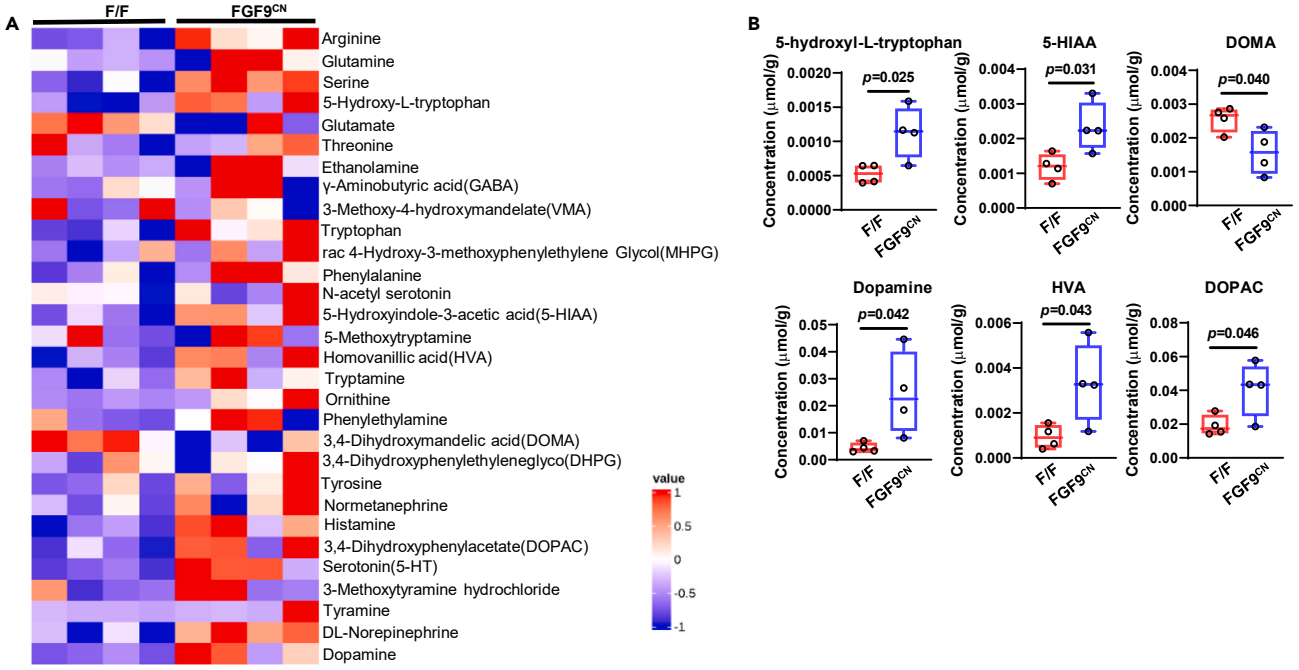

Figure 5. FGF9 deletion alters neurotransmitter release in cerebellum

(A) Extracted metabolites of cerebellum was analyzed by LC-MS/MS with multiple reaction monitoring (MRM) (n = 4). Heatmap depicting the 30 neurotransmitters in the cerebellum lysate of control and *Fgf9*^{cnGFAP} mice.

(B) Plots of statistically changed neurotransmitters (n = 4). Data are represented as Mean ± SD. Statistical analysis was performed using the unpaired two-tailed Student's *t* test. *, $p < 0.05$; F/F, *Fgf9*$^{f/f}$ control mice; FGF9^{CN}, *Fgf9*^{cnGFAP} mice.

activity is required for maintaining migration and alignment of Purkinje cell in cerebellum. The finding that the mutant Purkinje cells had high HVA and HIAA levels supports the idea that dopaminergic and serotoninergic signaling may underpin the ataxic defects.[27] FGF9 is proposed and excitation functions. Ablation of neuronal FGF9 results in defective Purkinje cell migration, poorly cellular organization in the PCL, incomplete IGL migration of granule cells, glial fiber breakage in BG cells, and amoeba-like shape in microglia (Figure 7B). Since Purkinje cells do not express GFAP, the FGF9 alleles remain intact in Purkinje cells in *Fgf9*^{cnGFAP} cerebellum. During the development of cerebellum, the function of Purkinje cells is extensively regulated by FGF9 derived from both autocrine and paracrine emitting from granule cells and Bergmann glia cells, which synchronously maintains the generation and correct positioning of BG (Figure 7C). However, whether the Purkinje defects were secondary effects due to abnormal BG radial fiber formation remains to be determined.

In summary, neuronal FGF9 is required for the development and function of Purkinje cells in the cerebellum. Loss of FGF9 in astrocytes, oligodendrocytes, and neurons leads to insufficient FGF9 during cerebellum development causes ataxia defects. Our findings thus reveal the specific pro-maturation, anti-inflammation and cell positioning functions of FGF9-mediated signaling in Purkinje cells and Bergmann glia cells. This is the first report providing the insights into the mechanism by which the FGF9 in cerebellum regulates alignment and function of Purkinje cells.

Limitations of the study

It is still unclear whether the Purkinje defects were secondary effects due to abnormal BG radial fiber formation. Subsequently, we need to focus on the issues mentioned above to determine the correlation of Purkinje cells and BG fibers.

STAR★METHODS

Detailed methods are provided in the online version of this paper and include the following:

- KEY RESOURCES TABLE
- RESOURCE AVAILABILITY
  - Lead contact
  - Materials availability
  - Data and code availability
- EXPERIMENTAL MODEL AND STUDY PARTICIPANT DETAILS

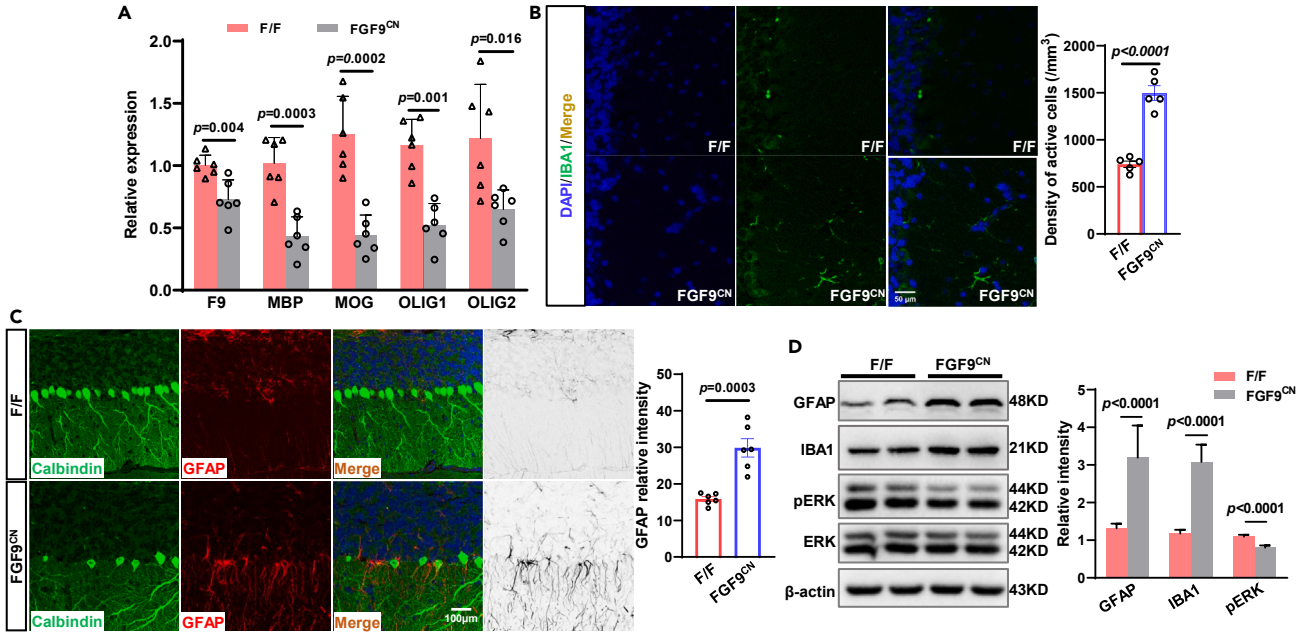

Figure 6. Ablation of FGF9 leads to mild neuroinflammation

(A) Myelination related genes expression detecting by real time RT-PCR in postnatal 7-day cerebella (n = 6). Results are shown as Mean ± SD. MBP, myelin basic protein; MOG, myelin oligodendrocyte glycoprotein; OLIG1, oligodendrocyte transcription factor 1; OLIG2, oligodendrocyte transcription factor 2.

(B) Immunofluorescence staining detecting the expression of IBA1 in mouse cerebellum (n = 5). All image analyses were performed blind to the experimental group. Confocal datasets were loaded into ImageJ. Cell density was normalized by the volume of cerebellum (area of DAPI/slice × stacks).

(C) Double immunofluorescence staining of Calbindin (Green) and GFAP (Red) in mouse cerebella (n = 6). Nuclei were counterstained with DAPI (blue).

(D) Western blotting showed the expression of GFAP, IBA1 and ERK (n = 5), β-actin was used as a loading control; relative intensity was calculated with ImageJ software. Data are represented as Mean ± SD. Statistical analysis was performed using the unpaired two-tailed Student's *t* test. *, p < 0.05; F/F, *Fgf9*$^{f/f}$ control mice; FGF9^{CN}, *Fgf9*^{cnGFAP} mice.

- Animals
- Primary astrocyte isolation and culture

- METHOD DETAILS
  - Motor coordination assessment
  - Ataxia assessments
  - Immunocytochemistry, immunohistochemistry, and nissl staining
  - Transmission electron microscopy
  - LC-MS/MS with multiple reaction monitoring (MRM) analyses
  - Electrophysiological recordings
  - Western blotting
  - Quantitative reverse transcription-polymerase chain reaction (qRT-PCR)
- QUANTIFICATION AND STATISTICAL ANALYSIS
  - Statistical analysis

SUPPLEMENTAL INFORMATION

Supplemental information can be found online at https://doi.org/10.1016/j.isci.2024.109039.

ACKNOWLEDGMENTS

This work was supported by the National Natural Science Foundation of China (82173013, 82372941, 81971894), the Natural Science Foundation of Zhejiang Province of China (LR20H310001, LWY20H300001), Project of Wenzhou Science & Technology Bureau (Y20210085).

AUTHOR CONTRIBUTIONS

W.C.: Conceptualization, Investigation, Resources, Writing-original draft, Writing-review and editing, Project administration, Funding acquisition. L.P.: Conceptualization, Resources, Funding acquisition. L.X.: Resources, Project administration. H.P.: Methodology, Software,

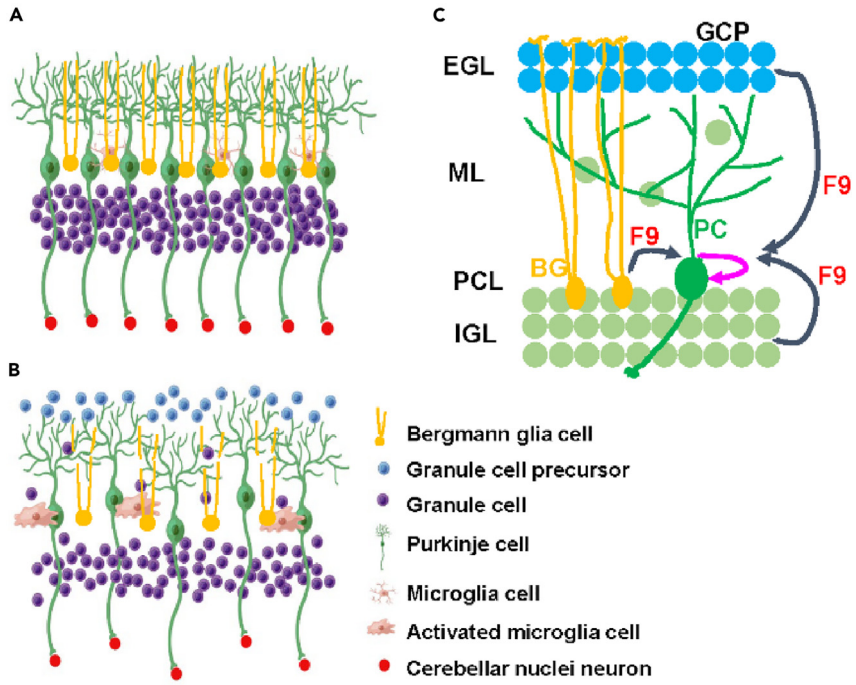

Figure 7. Schematic of the correlation between FGF9 and cerebellar neurons

(A) In adult *Fgf9*$^{f/f}$ control mouse cerebellum, Purkinje cells were arranged in a monolayer and transmitted information via axons to the deep cerebellar nuclei, Bergmann cells were regularly arranged in the Purkinje cell burst layer, and granule cells migrated to the inner granule layer by several hundred copies.

(B) FGF9 deletion in Glia and Bergman cells leads to Purkinje cell irregular arrangement, incomplete inner granular layer migration of granule cells, glial fiber breakage in Bergmann cells, and amoeba-like shape in microglia.

(C) Development and function of Purkinje cells need FGF9 derived from autocrine and paracrine.

Validation, Formal analysis, Data curation, Writing-original draft. Z.S.: Methodology, Validation, Data curation. L.S.: Methodology, Validation, Data curation. X.Z.: Methodology, Software, Validation. W.L.: Validation. H.Y.: Methodology, Formal analysis. X.D.: Methodology, Formal analysis; H.S.: Methodology, Formal analysis. The work reported in the paper has been performed by the authors, unless clearly specified in the text.

DECLARATION OF INTERESTS

The authors declare no competing interests

Received: September 19, 2023
Revised: November 28, 2023
Accepted: January 23, 2024
Published: January 26, 2024

REFERENCES

1. Ito, M. (2006). Cerebellar circuitry as a neuronal machine. Prog. Neurobiol. *78*, 272–303.
2. Lin, Y., Chen, L., Lin, C., Luo, Y., Tsai, R.Y.L., and Wang, F. (2009). Neuron-derived FGF9 is essential for scaffold formation of Bergmann radial fibers and migration of granule neurons in the cerebellum. Dev. Biol. *329*, 44–54. https://doi.org/10.1016/j.ydbio.2009.02.011.
3. Ruano, L., Melo, C., Silva, M.C., and Coutinho, P. (2014). The global epidemiology of hereditary ataxia and spastic paraplegia: a systematic review of prevalence studies. Neuroepidemiology *42*, 174–183. https://doi.org/10.1159/000358801.
4. Chopra, R., and Shakkottai, V.G. (2014). Translating cerebellar Purkinje neuron physiology to progress in dominantly inherited ataxia. Future Neurol. *9*, 187–196.
5. Akbar, U., and Ashizawa, T. (2015). Neurol. Clin. *33*, 225–248. https://doi.org/10.1016/j.ncl.2014.09.004.
6. Hui, Q., Jin, Z., Li, X., Liu, C., and Wang, X. (2018). FGF Family: From Drug Development to Clinical Application. Int. J. Mol. Sci. *19*, 1875. https://doi.org/10.3390/ijms19071875.
7. Itoh, N., Ohta, H., Nakayama, Y., and Konishi, M. (2016). Roles of FGF Signals in Heart Development, Health, and Disease. Front. Cell Dev. Biol. *4*, 110.
8. Basson, M.A., Echevarria, D., Ahn, C.P., Sudarov, A., Joyner, A.L., Mason, I.J., Martinez, S., and Martin, G.R. (2008). Specific regions within the embryonic midbrain and cerebellum require different levels of FGF signaling during development. Development (Cambridge, England) *135*, 889–898. https://doi.org/10.1242/dev.011569.
9. Chi, C.L., Martinez, S., Wurst, W., and Martin, G.R. (2003). The isthmic organizer signal

FGF8 is required for cell survival in the prospective midbrain and cerebellum. Development (Cambridge, England) *130*, 2633–2644.

10. Sotelo, C. (2004). Cellular and genetic regulation of the development of the cerebellar system. Prog. Neurobiol. *72*, 295–339.
11. Umemori, H., Linhoff, M.W., Ornitz, D.M., and Sanes, J.R. (2004). FGF22 and its close relatives are presynaptic organizing molecules in the mammalian brain. Cell *118*, 257–270.
12. Choi, G.E., Chae, C.W., Park, M.R., Yoon, J.H., Jung, Y.H., Lee, H.J., and Han, H.J. (2022). Prenatal glucocorticoid exposure selectively impairs neuroligin 1-dependent neurogenesis by suppressing astrocytic FGF2-neuronal FGFR1 axis. Cell. Mol. Life Sci. *79*, 294. https://doi.org/10.1007/s00018-022-04313-2.
13. Yaguchi, Y., Yu, T., Ahmed, M.U., Berry, M., Mason, I., and Basson, M.A. (2009). Fibroblast growth factor (FGF) gene expression in the developing cerebellum suggests multiple roles for FGF signaling during cerebellar morphogenesis and development. Dev. Dyn. *238*, 2058–2072. https://doi.org/10.1002/dvdy.22013.
14. Jiwani, T., Kim, J.J., and Rosenblum, N.D. (2020). Suppressor of fused controls cerebellum granule cell proliferation by suppressing Fgf8 and spatially regulating Gli proteins. Development *147*, dev170274. https://doi.org/10.1242/dev.170274.
15. Wang, S., Li, Y., Jiang, C., and Tian, H. (2018). Fibroblast growth factor 9 subfamily and the heart. Appl. Microbiol. Biotechnol. *102*, 605–613. https://doi.org/10.1007/s00253-017-8652-3.
16. Guo, M., Chen, H., Duan, W., Li, Z., Li, Y., Ma, Y., Xu, X., Yi, L., Bi, Y., Liu, Y., et al. (2020). FGF9 knockout in GABAergic neurons induces apoptosis and inflammation via the Fas/caspase-3 pathway in the cerebellum of mice. Brain Res. Bull. *154*, 91–101. https://doi.org/10.1016/j.brainresbull.2019.10.012.
17. Namiki, J., Suzuki, S., Masuda, T., Ishihama, Y., and Okano, H. (2012). Nestin protein is phosphorylated in adult neural stem/progenitor cells and not endothelial progenitor cells. Stem Cells Int. *2012*, 430138. https://doi.org/10.1155/2012/430138.
18. Popa, L.S., Streng, M.L., and Ebner, T.J. (2019). Purkinje Cell Representations of Behavior: Diary of a Busy Neuron. Neuroscientist *25*, 241–257. https://doi.org/10.1177/1073858418785628.
19. Nakamura, S., Todo, T., Motoi, Y., Haga, S., Aizawa, T., Ueki, A., and Ikeda, K. (1999). Glial expression of fibroblast growth factor-9 in rat central nervous system. Glia *28*, 53–65.
20. Fortin, D., Rom, E., Sun, H., Yayon, A., and Bansal, R. (2005). Distinct fibroblast growth factor (FGF)/FGF receptor signaling pairs initiate diverse cellular responses in the oligodendrocyte lineage. J. Neurosci. *25*, 7470–7479. https://doi.org/10.1523/JNEUROSCI.2120-05.2005.
21. Garces, A., Nishimune, H., Philippe, J.M., Pettmann, B., and deLapeyriere, O. (2000). FGF9: a motoneuron survival factor expressed by medial thoracic and sacral motoneurons. J. Neurosci. Res. *60*, 1–9. https://doi.org/10.1002/(SICI)1097-4547.
22. Sotelo, C. (2015). Molecular layer interneurons of the cerebellum: developmental and morphological aspects. Cerebellum *14*, 534–556. https://doi.org/10.1007/s12311-015-0648-x.
23. Hibi, M., and Shimizu, T. (2012). Development of the cerebellum and cerebellar neural circuits. Dev. Neurobiol. *72*, 282–301. https://doi.org/10.1002/dneu.20875.
24. White, J.J., and Sillitoe, R.V. (2013). Development of the cerebellum: from gene expression patterns to circuit maps. Wiley Interdiscip. Rev. Dev. Biol. *2*, 149–164. https://doi.org/10.1002/wdev.65.
25. Apps, R., and Garwicz, M. (2005). Anatomical and physiological foundations of cerebellar information processing. Nat. Rev. Neurosci. *6*, 297–311.
26. Capes-Davis, A., Tolhurst, O., Dunn, J.M., and Jeffrey, P.L. (2005). Expression of doublecortin (DCX) and doublecortin-like kinase (DCLK) within the developing chick brain. Dev. Dyn. *232*, 457–467. https://doi.org/10.1002/dvdy.20240.
27. Papandreou, A., Rahman, S., Fratter, C., Ng, J., Meyer, E., Carr, L.J., Champion, M., Clarke, A., Gissen, P., Hemingway, C., et al. (2018). Spectrum of movement disorders and neurotransmitter abnormalities in paediatric POLG disease. J. Inherit. Metab. Dis. *41*, 1275–1283. https://doi.org/10.1007/s10545-018-0227-7.
28. Zhuo, L., Theis, M., Alvarez-Maya, I., Brenner, M., Willecke, K., and Messing, A. (2001). hGFAP-cre transgenic mice for manipulation of glial and neuronal function in vivo. Genesis *31*, 85–94.
29. Lin, Y., Liu, G., and Wang, F. (2006). Generation of an Fgf9 conditional null allele. Genesis *44*, 150–154.
30. Soriano, P. (1999). Generalized lacZ expression with the ROSA26 Cre reporter strain. Nat. Genet. *21*, 70–71.
31. Lin, Y., Liu, G., Zhang, Y., Hu, Y.P., Yu, K., Lin, C., McKeehan, K., Xuan, J.W., Ornitz, D.M., Shen, M.M., et al. (2007). Fibroblast growth factor receptor 2 tyrosine kinase is required for prostatic morphogenesis and the acquisition of strict androgen dependency for adult tissue homeostasis. Development *134*, 723–734.
32. Trokovic, R., Trokovic, N., Hernesniemi, S., Pirvola, U., Vogt Weisenhorn, D.M., Rossant, J., McMahon, A.P., Wurst, W., and Partanen, J. (2003). FGFR1 is independently required in both developing mid- and hindbrain for sustained response to isthmic signals. EMBO J. *22*, 1811–1823.
33. Weinstein, M., Xu, X., Ohyama, K., and Deng, C.X. (1998). FGFR-3 and FGFR-4 function cooperatively to direct alveogenesis in the murine lung. Development *125*, 3615–3623.
34. Watase, K., Gatchel, J.R., Sun, Y., Emamian, E., Atkinson, R., Richman, R., Mizusawa, H., Orr, H.T., Shaw, C., and Zoghbi, H.Y. (2007). Lithium therapy improves neurological function and hippocampal dendritic arborization in a spinocerebellar ataxia type 1 mouse model. PLoS Med. *4*, e182.
35. Luong, T.N., Carlisle, H.J., Southwell, A., and Patterson, P.H. (2011). Assessment of motor balance and coordination in mice using the balance beam. J. Vis. Exp. 2376. https://doi.org/10.3791/2376.
36. Guyenet, S.J., Furrer, S.A., Damian, V.M., Baughan, T.D., La Spada, A.R., and Garden, G.A. (2010). A simple composite phenotype scoring system for evaluating mouse models of cerebellar ataxia. J. Vis. Exp. 1787. https://doi.org/10.3791/1787.
37. Schuster, K.H., Putka, A.F., and McLoughlin, H.S. (2022). Pathogenetic Mechanisms Underlying Spinocerebellar Ataxia Type 3 Are Altered in Primary Oligodendrocyte Culture. Cells *11*, 2615. https://doi.org/10.3390/cells11162615.
38. Choi, Y.S., and Lee, K.H. (2016). Multiple reaction monitoring assay based on conventional liquid chromatography and electrospray ionization for simultaneous monitoring of multiple cerebrospinal fluid biomarker candidates for Alzheimer's disease. Arch Pharm. Res. (Seoul) *39*, 390–397. https://doi.org/10.1007/s12272-015-0663-y.

STAR★METHODS

KEY RESOURCES TABLE

REAGENT or RESOURCE	SOURCE	IDENTIFIER
Antibodies		
anti-IBA1	Wako	Cat#19741; RRID: AB_839504
anti-GFAP	Cell Signaling Technology	Cat#12389; RRID: AB_2631098
anti-Calbindin	Cell Signaling Technology	Cat#2173; RRID: AB_2183553
anti-DCX	Cell Signaling Technology	Cat#46404; RRID: AB_561007
anti-FGF9	Cell Signaling Technology	Cat#9740; RRID: AB_2853187
anti-pERK	Cell Signaling Technology	Cat#3192; RRID: AB_2095847
anti-ERK	Cell Signaling Technology	Cat#3179; RRID: AB_2095853
anti-IL-6	Santa Cruz Biotechnology	Cat#28343; RRID: AB_627805
anti-TNF-α	Santa Cruz Biotechnology	Cat#12744; RRID: AB_628372
anti-IL-1β	Santa Cruz Biotechnology	Cat#12742; RRID: AB_627791
anti-β-actin	Santa Cruz Biotechnology	Cat#47778; RRID: AB_626632
anti-CA8	Santa Cruz Biotechnology	Cat#166626; RRID: AB_2066290
anti-NeuN	Millipore	Cat#377; RRID: AB_2298772
Alexa Fluor 488	Thermo Fisher Scientific	Cat#11034
Alexa Fluor 568	Thermo Fisher Scientific	Cat#11004
Chemicals, peptides, and recombinant proteins		
DAPI	Cell Signaling Techonology	Cat#3192
Biocytin	Thermo Fisher Scientific	Cat#1603
RIPA buffer	Thermo Fisher Scientific	Cat#89901
phenylmethylsulphonyl fluoride (PMSF)	Applygen	Cat#1055
Protease and Phosphatase Inhibitor	Applygen	Cat#1261
SYBR green reagent	Roche	Cat#4913914001
TRIzol reagent	Invitrogen	Cat#15596026
Critical commercial assays		
Bicinchoninic acid (BCA) Protein Assay Kit	Thermo Scientific	Cat#55860
DAB staining kit	MX biotechnologies	Cat#0071
The UltraSensitive SP kit	MX biotechnologies	Cat#9710
Nissl stain kit	Beyotime	Cat#0070
Experimental models: Organisms/strains		
Fgf9$^{f/f}$ and *Fgf9*^{cnGFAP} mice	Jackson Lab	IMSR_JAX:004600
Oligonucleotides		
Fgf 9-Forward: ATGGCTCCCTTAGGTGAAGTT	This paper	N/A
Fgf 9-Reverse: TCATTTAGCAACACCGGACTG	This paper	N/A
Mbp- Forward: TCACAGCGATCCAAGTACCTG	This paper	N/A
Mbp-Reverse: CCCCTGTCACCGCTAAAGAA	This paper	N/A
Mog-Forward: TCATGCAGCTATGCAGGACAA	This paper	N/A

(*Continued on next page*)

Continued

REAGENT or RESOURCE	SOURCE	IDENTIFIER
Mog-Reverse: TTTCGGTAGAGGTGAACCACT	This paper	N/A
Olig 1-Forward: TCTTCCACCGCATCCCTTCT	This paper	N/A
Olig1-Reverse: CCGAGTAGGGTAGGATAACTTCG	This paper	N/A
Olig 2-Forward: GGCGGTGGCTTCAAGTCAT	This paper	N/A
Olig 2-Reverse: CATGGCGATGTTGAGGTCG	This paper	N/A
Software and algorithms		
GraphPad Prism 8.0.2.263	GraphPad Software	https://www.graphpad.com/
ImageJ	NIH	RRID: SRC_003070
Adobe Illustrator	Adobe	https://www.adobe.com/

RESOURCE AVAILABILITY

Lead contact

Further information and requests for resources and reagents should be directed to and will be fulfilled by the lead contact: Cong Wang (cwang@wmu.edu.cn).

Materials availability

Mouse generated in this study are available from the lead contact upon request.

Data and code availability

- Any additional information required to reanalyze the data reported in this paper is available from the lead contact upon request.
- This paper analyzes existing, publicly available data. These accession numbers for the datasets are listed in the key resources table.
- The paper does not report any original code.

EXPERIMENTAL MODEL AND STUDY PARTICIPANT DETAILS

Animals

All animals were housed under the Program of Animal Resources of the Wenzhou Medical University in accordance with the principles and procedures of the Guide for the Care and Use of Laboratory Animals. All experimental procedures were approved by the Institutional Animal Care and Use Committee. The mice carrying LoxP-flanked *Fgf9* (*Fgf9*^{flox}), and the hGFAP-Cre transgenic mice specific for glia and neuron (IMSR_JAX:004600),[28] were bred as described in.[29] Genotypes of the mice bearing the *floxed*, conditional null, and wildtype *Fgf9*, as well as the Cre driver were determined by PCR analyses as described in.[29–33] All experiments were performed using 3-month-old male mice unless clearly labeled.

Primary astrocyte isolation and culture

Dissected the brain tissue from newborn *Fgf9*$^{f/f}$ and *Fgf9*^{cnGFAP} mice (within 24 h of birth), and then minced the brain in cold PBS to wash for removing blood stains. After gently brush away the meninges and blood vessels on the surface of the brain, cut the brain to small pieces and digested thoroughly with 0.05% trypsin and 0.1% DNase I for 10 min at 37°C, which was terminated with DMEM/F12 culture medium containing 10% fetal bovine serum, 100 U/mL penicillin and 100 μg/mL streptomycin (Gibco, Carlsbad, CA, USA). Pipette the mixture to blow the cells into single-cell suspension followed by centrifuging for 5 min at 1000 rpm/min. The cells were cultured with DMEM/F12 complete medium in 5% CO_2 incubators, then the medium was gently aspirated to a different dish after 3 h to get rid of the adhering fibroblasts, recombinant human FGF9 was added to the culture medium at a final concentration of 20 ng/mL for 48 h to detect the astrocyte morphology.

METHOD DETAILS

Motor coordination assessment

The rotarod test was performed using a modified protocol.[34] Experimental mice were trained to keep their balance on a rotarod with a constant speed (10 rpm/min). Mice were subsequently monitored on an accelerating rotarod (10~50 rpm over 180s). The latency to fall off the rod

was recorded. The mice were given 3 trials per day for 3 consecutive days. The balance beam test was performed as previously described.[35] Experimental mice were trained to walk across the raised beam (60 cm in length, 1.0 cm in diameter) 2 times. Each mouse was given three trials, other, the cross latency and foot slip number were recorded in each trial. Either the left or right hind paw slipping off the beam is recognized as one footslip.

Ataxia assessments

The assessments included hindlimb clasping, ledge test, gait and kyphosis, with individual measure scored on a scale of 0–3 and a combined total of 0–12 for all four measures. 0 represents relevant phenotype absence and 3 designates the most severe defects. As a protection against bias, the persons operating the assessments were blind to mouse genotypes. Each test was conducted numerous times to ensure reproducibility.[36]

Immunocytochemistry, immunohistochemistry, and nissl staining

The freshly dissected brains were fixed with PFA overnight, followed by series dehydration with ethanol and sectioned (5-μm thickness). After rehydration and antigen retrieval in the citrate buffer, the sections were incubated with 5%BSA at 4°C overnight, followed by incubation with primary antibodies at 4°C overnight, and then secondary antibodies as describe previously.[37] The source and dilution of the antibodies are anti-IBA1 (1/200; Wako), anti-CA8 (1/50; Santa Cruz), anti-GFAP (1/500; Cell Signaling), anti-Calbindin (1/200, CST), anti-DCX (1/1000; CST), anti-NeuN (1/1000; Millipore), goat anti-mouse IgG conjugate Alexa Fluor 488 (Thermo Fisher, 1/500), and Alexa Fluor 568 (Thermo Fisher, 1/500). DAPI (CST, H-1200) was used for nuclear counterstaining. Fluorescent images were captured with a laser confocal microscope (Leica SP8).

For IHC staining, the sections were rehydrated, antigen retrieval, and then incubated with 3% hydrogen peroxide for 10 min at room temperature to quench endogenous peroxidase. The sections were then incubated with the primary antibodies anti-FGF9 (1/250; Cell Signaling, No. 2586S) at 4°C overnight, followed by incubation with biotinylated secondary antibodies for 10 min at room temperature. After a thorough wash, the sections were incubated with Streptavidin-Peroxidase. The UltraSensitive SP kit (mouse/rabbit) and a DAB staining kit (MXB biotechnologies) were used for the visualization according to the manufacturer's protocol. Hematoxylin staining were used for counterstaining. For Nissl staining, the sections were stained with a Nissl stain (crystal violet, Beyotime, Nanjing, China) for 20 min at room temperature. Images were collected with a Motic virtual microscope (Nikon).

Transmission electron microscopy

Tissue processing was performed as described previously.[37] Briefly, the cerebella were fixed with 2.5% glutaraldehyde in 0.1M PBS (pH 7.4) at 4°C for 2.5 h, washed three times with 0.1M PBS, and postfixed in 1% OsO4 at 4°C for 2 h. The samples were subsequently series dehydrated with ethanol solutions: 15 min in 30% ethanol, 15 min in 50% ethanol, 15 min in 70% ethanol, 15 min in 90% ethanol, and 2 × 20 min in 100% ethanol. The tissues were then embedded in Spurr's resin, and ultrathin (60 nm) sectioned. The sections were collected with a copper grid, stained with either uranyl acetate or lead citrate, and examined with an HT-7800 transmission electron microscope (Hitachi).

LC-MS/MS with multiple reaction monitoring (MRM) analyses

Tissue samples were digested, extracted, and analyzed as described.[38] To extract metabolites from tissue samples, 800 μL of cold acetonitrile (containing 1% formic acid) extraction solvent was added to 80 mg sample, and adequately vortexed. The lysate was homogenized by MP homogenizer (24 × 2, 6.0 M/S, 60 s, twice) and sonicated at 4°C (30 min/once, twice) then centrifuged at 14,000 g for 20 min at 4°C and the supernatant was dried in a vacuum centrifuge at 4°C. Then the samples were re-dissolved in 100 μL acetonitrile/water (1:1, v/v) solvent for LC-MS analysis. A Sciex 5500 Q-Trap mass spectrometer equipped with an electrosprayionization (ESI) source was used for the analyses of NTs. The mass spectrometer was coupled with an Agilent 1290 infinity UHPLC system. Quality control (QC) samples were set for each interval of experimental samples in the sample queue.

Chromatographic peak area and retention time was monitored by Multiquant software.[1] Metabolites with fold changes >1.5 or fold changes <0.67 were considered as the significantly changed metabolites. For hierarchical clustering, Cluster3.0 (http://bonsai.hgc.jp/%mdehoon/software/cluster/software.htm) and the Java Treeview software (http://jtreeview.sourceforge.net) were used. Euclidean distance algorithm for similarity measure and average linkage clustering algorithm (clustering uses the centroids of the observations) for clustering were selected when performing hierarchical clustering.

Electrophysiological recordings

Brains with cerebellum were placed in an ice-cold and oxygenated high sucrose slicing solution (234 mM sucrose, 11 mM glucose, 26 mM $NaHCO_3$, 2.5 mM KCl, 1.25 mM NaH_2PO_4, 10 mM $MgSO_4$, and 0.5 mM $CaCl_2$) for 2–3 min. Parasagittal cerebellar slices (300-μm thick) were sectioned in slicing solution using a Leica VT1200S vibratome and recovered at 34°C for 1 h in the oxygen-saturated artificial cerebral spinal fluid (ACSF) containing the following chemicals:126 mM NaCl, 26 mM $NaHCO_3$, 10 mM glucose, 2.5 mM KCl, 1.25 mM NaH_2PO_4, 2 mM $MgCl_2$, and 2 mM $CaCl_2$ (pH 7.4). In a recording chamber, cerebellar slices were placed and visualized with a fixed-staged upright microscope (Olympus MVX10). All recordings of Purkinje cells were performed with EPC-10 Patchmaster (HEKA, Germany), and with continuous ACSF perfusion (2 mL/min at 33°C, controlled by an Automatic Temperature Controller, Warner Instruments, Hamden, CT), Glass pipettes

(nonfilament, Garner Glass Company, CA, USA) were pulled (Model P-97, Sutter Instruments) to obtain electrodes that generated resistances between 5 and 7 MΩ after being filled with intracellular solution containing 130 mM K-gluconate, 10 mM KCl, 10 mM HEPES, 4 mM Mg-ATP, 0.3 mM Na-GTP, and 10 mM Phosphocreatine.

To record the spontaneous firing frequency, the Purkinje cells were recorded under cell-attached mode with holding potential set as 0 mV and each cell will be recorded for at least 5 min. For electrophysiological recordings in whole-cell configuration, a giga-ohm seal between the cell and the glass pipette was formed first, and a brief suction was applied to break into the cell. Purkinje cell action potential firing properties were recorded under current clamp mode. In order to investigate the morphology of each recorded Purkinje cell, biocytin (1%, B1592, ThermoFisher Scientific) was added to the intracellular solution, and cells were kept under whole cell recording mode for at least 10 min, allowing the biocytin to diffuse well into the cell. Slices containing recorded cells were then fixed with 4% paraformaldehyde overnight and processed for *post-hoc* morphological characterization. All data were transferred to abf files and analyzed using Clampfit 10.6 software.

Western blotting

Cells were homogenized and lysed with RIPA buffer (Thermo Scientific, MA, USA) containing a 1%phenylmethylsulfonyl fluoride (PMSF) and 1% protein phosphatase inhibitor mixture (Applygen, Beijing, China). The extracted proteins were harvested by centrifugation (12,000×g, 15 min, 4°C). Protein concentration was determined using the bicinchoninic acid (BCA) Protein Assay Kit (Thermo Scientific, MA, USA). Twenty micrograms of the extracted protein from each sample was subjected to electrophoresis in 8–12% SDS-PAGE depending on the molecular weight of the protein. Proteins in the gels were transferred onto polyvinylidene difluoride (PVDF) membranes (EDM Millipore, MA, USA) for Western blot analysis with the indicated antibodies. The sources of the antibodies and dilutions are as follows: anti-IBA1 (1:1000), anti-pERK (1:1000), anti-ERK (1:1000), and anti-GFAP (1:1000) were obtained from Cell Signaling Technology (Beverly, MA, USA); anti-β-actin (1:1000), anti-IL-6 (1:1000), anti-TNF-α (1:1000) and anti-IL-1β (1:1000), were all purchased from Santa Cruz Biotechnology (CA,USA). The ECL Plus chemiluminescent reagent (Thermo Scientific, MA, USA) was used to visualize the proteins. Protein bands were quantitated by ImageJ (NIH, USA).

Quantitative reverse transcription-polymerase chain reaction (qRT-PCR)

Total RNA was extracted using the TRIzol reagent (Invitrogen) according to the manufacturer's instructions. Reverse transcription was performed using the Super-Script III Reverse Transcriptase kit (TOYOBO). The qRT-PCR analysis was carried out with the ROCHE 480 Real-Time Light Cycler system and SYBR green reagent (Roche, No. 4913914001). The primer sequences are shown in key resources table. All results presented were calculated from CT values derived from the qRT-PCR.

QUANTIFICATION AND STATISTICAL ANALYSIS

Statistical analysis

All statistical values are presented as the Means ± SD. Statistical analyses were conducted by SPSS software version 21.0 (SPSS Inc., IL, USA). Significant differences were assessed by Student's test (two-tailed), and two-way ANOVA with the post hoc Tukey's test. Spearman rank correlation was used to analyze the non-normally distributed data. $P < 0.05$ was considered statistically significant.